

STAG: Structural Test-time Alignment of Gradients for Online Adaptation

Juhyeon Shin¹ Yujin Oh² Jonghyun Lee³ Saehyung Lee⁴ Minjun Park¹ Dongjun Lee⁵ Uiwon Hwang²
Sungroh Yoon¹

Abstract

Test-Time Adaptation (TTA) adapts pre-trained models using only unlabeled test streams, requiring real-time inference and update without access to source data. We propose **Structural Test-time Alignment of Gradients (STAG)**, a lightweight **plug-in enhancer** that exploits an always-available structural signal: the classifier’s intrinsic geometry. STAG derives class-wise *structural anchors* from classifier weights via self-structural entropy, and during adaptation analytically computes the predicted-class entropy gradient from forward-pass quantities, aligning it to the corresponding anchor with a cosine-similarity loss. This closed-form design incurs near-zero memory and latency overhead and requires no additional backpropagation beyond the underlying baseline. Across corrupted image classification and continual semantic segmentation, STAG provides broadly applicable performance gains for strong TTA baselines on both CNN and Transformer architectures regardless of the underlying normalization scheme, with particularly large gains under challenging online regimes such as imbalanced label shifts, single-sample adaptation, mixed corruption streams and long-horizon continual TTA.

1. Introduction

Deep networks are typically trained under the assumption that train and test distributions match (Krizhevsky et al., 2017), yet real-world corruptions (e.g., adverse weather and natural distortions) often violate this assumption and can severely degrade performance (Hendrycks & Dietterich, 2019). While prior adaptation/generalization methods have

¹Seoul National University, Seoul, Republic of Korea ²Division of Artificial Intelligence & Software, Ewha Womans University, Seoul, Republic of Korea ³KRAFTON, Seoul, Republic of Korea

⁴Microsoft, Redmond, WA, USA ⁵Georgia Institute of Technology, Atlanta, GA, USA. Correspondence to: Uiwon Hwang <uiwon.hwang@ewha.ac.kr>, Sungroh Yoon <sryoon@snu.ac.kr>.

Preprint. February 9, 2026.

been studied extensively (Csurka, 2017; Muandet et al., 2013; Ganin & Lempitsky, 2015; Liang et al., 2020; Lee et al., 2022; Hwang et al., 2024), many require source data access or costly offline adaptation stages.

Test-Time Adaptation (TTA) has emerged as a more practical paradigm, adapting models on-the-fly using only unlabeled test streams. Unlike standard domain adaptation, TTA operates under extreme information scarcity: target labels are unavailable, source data are typically inaccessible, and the target distribution may evolve over time. Moreover, adaptation must be performed online, interleaved with inference, since predictions are required continuously while the model is being updated on the same incoming stream. These constraints make test-time learning fundamentally different from offline finetuning and place a premium on methods that are lightweight, stable, and compatible with real-world deployment budgets.

In this work, we focus on a source of signal that remains always available in information-scarce TTA: the model’s classifier geometry. Even when target labels and source data are absent, the classifier weights still encode class-specific structure learned during source training. Concretely, if we treat each class weight vector as a virtual input and pass it through the classifier, we observe a strikingly consistent pattern of structural correctness—each weight strongly matches its own class—across diverse architectures and normalization schemes. This suggests that, while test-time predictions and confidence may fluctuate under distribution shift, the classifier can still provide a stable structural prior. We formalize this intuition via self-structural entropy and use it to derive class-wise reference directions that can guide online updates without requiring any additional supervision.

Based on this, we propose **Structural Test-time Alignment of Gradients (STAG)**, a plug-and-play regularizer applicable to arbitrary TTA objectives. STAG (i) extracts class-specific structural anchors from classifier weights in closed form before adaptation, and (ii) during online adaptation, aligns the predicted-class entropy gradient with the corresponding anchor via a cosine-similarity loss, weighted by a decaying coefficient. Both components admit efficient analytical forms, adding negligible overhead and requiring no additional backpropagation beyond the underlying baseline.

We evaluate STAG on image classification (ImageNet-C,

CIFAR-10/100-C) and semantic segmentation (Cityscapes-ACDC) across CNNs and Transformers with diverse normalization schemes. STAG delivers robust performance enhancements under both stationary and dynamic shifts, including single-sample adaptation, label imbalance, mixed corruption streams and long-horizon continual TTA, while maintaining near-zero latency. The primary contributions of this work are summarized as follows:

- **Plug-and-play Regularization:** We propose **STAG**, a broadly applicable **plug-in enhancer** for online test-time adaptation. STAG exploits always-available *classifier structure* to supply an additional, architecture-agnostic signal that can be seamlessly combined with existing TTA objectives.
- **Analytical Efficiency:** STAG admits a **closed-form** formulation for computing structural anchors and the associated alignment signal, incurring **near-zero** memory and latency overhead. This makes it practical for real-time online deployment without introducing additional backpropagation beyond the underlying baseline.
- **Architecture-Agnostic Robustness:** We validate STAG across both CNNs and Transformers with diverse normalization schemes (BN, GN, LN), and demonstrate that STAG yields significant performance improvements across a broad spectrum of scenarios, encompassing imbalanced label shifts, single-sample adaptation, mixed corruption settings and long-horizon continual TTA.

2. Related Work

Test-Time Adaptation (TTA) updates a deployed model on-the-fly using only an unlabeled test stream, while maintaining tight latency and memory budgets. To satisfy these constraints, many methods adapt only lightweight components such as normalization statistics or affine parameters at test time (Schneider et al., 2020). A widely used learning signal is *entropy minimization*, exemplified by TENT (Wang et al., 2021) and its efficient variant EATA (Niu et al., 2022). More recent baselines such as SAR (Niu et al., 2023) and DeYO (Lee et al., 2024) further improve robustness by incorporating additional regularization and/or sample filtering mechanisms on top of entropy-based adaptation. Beyond the standard setting, *continual* TTA considers long, non-stationary test streams where the distribution changes over time and naïve online updates can accumulate errors and cause forgetting; methods such as CoTTA (Wang et al., 2022) and EcoTTA (Song et al., 2023) explicitly target stability over extended horizons by introducing temporal ensembling and/or consistency-based regularization across test-time states. In contrast to proposing another standalone objective, we present **STAG** as a lightweight *plug-in enhancer* that can be seamlessly combined with these TTA baselines by exploiting an always-available structural signal from the classifier geometry to guide online updates.

3. Structural Test-time Alignment of Gradients

3.1. Preliminaries

Problem Setup We consider the task of **Test-Time Adaptation (TTA)**, where a model pre-trained on a source domain is adapted to an unseen target domain without any access to the original source data. Let the source training and target test datasets be denoted as $\mathcal{D}_{\text{tr}} = \{(\mathbf{x}_i^{\text{tr}}, y_i^{\text{tr}}) : \mathbf{x}_i^{\text{tr}} \sim P(\mathcal{X}), y_i^{\text{tr}} \in \mathcal{Y}\}$ and $\mathcal{D}_{\text{te}} = \{(\mathbf{x}_i^{\text{te}}, y_i^{\text{te}}) : \mathbf{x}_i^{\text{te}} \sim Q(\mathcal{X}), y_i^{\text{te}} \in \mathcal{Y}\}$, respectively. In the TTA setting, we encounter a distribution shift $P(\mathcal{X}) \neq Q(\mathcal{X})$ while the target labels y_i^{te} remain strictly unavailable during the online adaptation process. Both domains are assumed to share a common label space $\mathcal{Y} = \{1, \dots, c\}$ consisting of c distinct classes. This setup poses a fundamental challenge: the model must effectively mitigate the domain gap by maximizing the utility of its internal knowledge under extreme information scarcity.

Model Architecture The model consists of a feature extractor $f_{\phi} : \mathcal{X} \rightarrow \mathcal{H}$ with parameters ϕ , which maps input data to a D -dimensional feature space $\mathcal{H} \subseteq \mathbb{R}^D$. This is followed by a classifier $g_{\mathbf{w}} : \mathcal{H} \rightarrow \mathbb{R}^c$ parameterized by $\mathbf{w} = \{\mathbf{b}, \mathbf{w}_1, \dots, \mathbf{w}_c\}$. Each weight vector $\mathbf{w}_k \in \mathbb{R}^D$ corresponds to class $k \in \{1, \dots, c\}$ and encapsulates the semantic representation of that category. For a given input \mathbf{x} , the model generates a feature representation $\mathbf{h} = f_{\phi}(\mathbf{x}) \in \mathcal{H}$ and a subsequent logit vector $\mathbf{z} = g_{\mathbf{w}}(\mathbf{h}) \in \mathbb{R}^c$. The final prediction probability $\mathbf{p} = \sigma(\mathbf{z})$ is obtained via the softmax function $\sigma(\cdot)$, where the k -th element is defined as $p_k = \exp(z_k) / \sum_{j=1}^c \exp(z_j)$.

Online Test-Time Adaptation During the online adaptation phase, test samples $\{\mathbf{x}_t^{\text{te}}\}$ arrive sequentially, and the model updates a subset of its parameters $\theta_{\text{adapt}} \subseteq \{\phi, \mathbf{w}\}$. Due to the absence of ground-truth labels in the target domain, it is standard practice (Wang et al., 2021; Niu et al., 2022; 2023; Lee et al., 2024) to minimize an unsupervised objective such as the Shannon entropy loss \mathcal{L}_{ent} :

$$\mathcal{L}_{\text{ent}}(\mathbf{x}) = - \sum_{i=1}^c p_i \ln p_i. \quad (1)$$

Rather than relying solely on the instantaneous entropy gradient, we propose a geometric regularizer that aligns the adaptation direction with structural anchors derived from the classifier’s own weights. By providing a reference based on the classifier’s intrinsic geometry, this alignment mechanism maximizes the utility of internal information and facilitates the formation of a feature space that remains semantically compatible with the classifier’s decision logic.

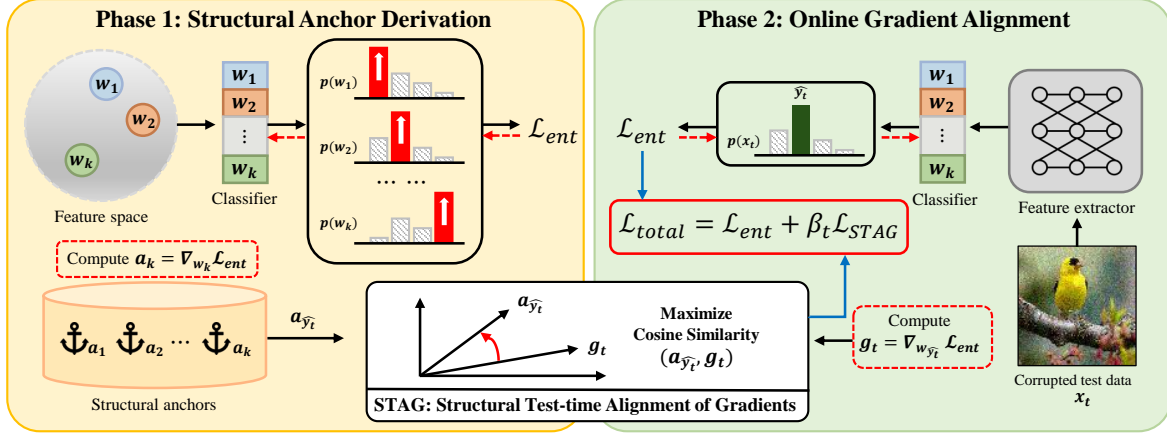


Figure 1. The Overall Framework of STAG. (a) Phase 1: Structural Anchor Derivation. We derive structural anchors \mathbf{a}_k by calculating the gradient of self-structural entropy from the classifier weights. (b) Phase 2: Online Gradient Alignment. During test-time adaptation, STAG analytically computes the online entropy gradient g_t from test samples and aligns it with the corresponding structural anchor $\mathbf{a}_{\hat{y}_t}$.

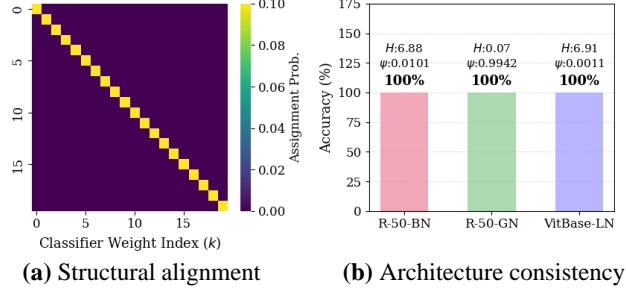


Figure 2. Validation of classifier weights as structural anchors. (a) Softmax assignment probability heatmap for 20 selected ImageNet classes (ResNet50-GN). (b) Metric consistency across architectures: ResNet50-BN, ResNet50-GN and VitBase-LN. H , ψ , and Acc denote self-entropy, mean diagonal probability (MDP), and structural accuracy, respectively.

3.2. Methodology

In this section, we present the details of **Structural Test-time Alignment of Gradients (STAG)**. STAG implements a two-phase process: (i) extracting structural anchors derived from the classifier weights, and (ii) aligning the online gradients with these anchors to guide the adaptation. The overall framework is illustrated in Figure 1.

Anchor Extraction from Self-structural Entropy STAG treats the classifier weights $\{w_1, \dots, w_c\}$ as meaningful proxies for the semantic structure of the feature space. To justify this, we analyze the structural consistency by treating each weight vector w_k as a virtual input to the classifier. As shown in Figure 2(a), the softmax heatmap for 20 sampled classes from a ResNet50-GN pretrained on ImageNet exhibits a sharp diagonal, confirming that each weight is correctly mapped to its respective category. Furthermore, our evaluation across various architectures—including ResNet with Batch Normalization (BN), Group Normalization (GN),

and ViT with Layer Normalization (LN)—reveals that even when the mean diagonal probability (ψ) is low or self-entropy (H) is high, the *structural accuracy* remains consistently at 100% (see Figure 2(b)). This 100% accuracy demonstrates that the classifier weights, despite differing in their probabilistic confidence, preserve the essential semantic boundaries of the inherent classifier geometry.

Based on this insight, we extract the structural relationships by defining an **inter-class similarity matrix** $\mathbf{Z} \in \mathbb{R}^{c \times c}$. Each element Z_{kj} represents the logit value for the j -th class when the k -th class weight w_k is used as a virtual input to the classifier:

$$Z_{kj} = \mathbf{w}_j^\top \mathbf{w}_k + b_j, \quad (2)$$

where b_j is the bias term corresponding to the j -th class. Then we calculate the **self-structural entropy** H_k :

$$H_k = - \sum_{j=1}^c p_{kj} \ln p_{kj}, \quad (3)$$

where $p_{kj} = \sigma(\mathbf{Z}_k)_j$ is the softmax probability.

The structural anchor \mathbf{a}_k is then derived by isolating the **self-structural sensitivity**, which represents the most dominant directional component for minimizing structural ambiguity. While the full gradient of entropy involves a linear combination of all weights, we focus on the sensitivity of the k -th class with respect to its own prototype to ensure a de-noised and class-specific guidance. Specifically, \mathbf{a}_k is formulated in an analytical closed-form as follows:

$$\mathbf{a}_k = s_k \mathbf{w}_k, \quad \text{where } s_k = -p_{kk}(\ln p_{kk} + H_k). \quad (4)$$

Here, the **structural sensitivity** s_k captures the internal gradient magnitude that stabilizes the k -th decision boundary. Detailed derivation of this component is provided in

Appendix A. This self-referential formulation ensures both computational efficiency and stable adaptation by filtering out gradient interference from unrelated classes.

Sample-wise Gradient Extraction During the online adaptation stage, STAG identifies the instantaneous update direction for each arriving test sample \mathbf{x}_t . Specifically, we first obtain the feature representation $\mathbf{h}_t = f_\phi(\mathbf{x}_t) \in \mathbb{R}^D$ and the predicted class $\hat{y}_t = \arg \max_k p_{tk}$ through a standard forward pass. To determine the model’s adaptation intent, we extract the gradient of the entropy loss \mathcal{L}_{ent} with respect to the weight vector of the predicted class, $\mathbf{w}_{\hat{y}_t}$. Following the analytical derivation in Appendix A, the **logit-level sensitivity** s_t for the sample is defined as:

$$s_t = \frac{\partial \mathcal{L}_{\text{ent}}}{\partial z_{t, \hat{y}_t}} = -p_{t, \hat{y}_t} (\ln p_{t, \hat{y}_t} + H(\mathbf{p}_t)), \quad (5)$$

where $H(\mathbf{p}_t)$ is the predictive entropy of the current sample. The resulting **online gradient** \mathbf{g}_t , which represents the sample-driven adaptation direction in the weight geometry, is then formulated as:

$$\mathbf{g}_t = \nabla_{\mathbf{w}_{\hat{y}_t}} \mathcal{L}_{\text{ent}} = s_t \cdot \mathbf{h}_t. \quad (6)$$

This closed-form formulation allows \mathbf{g}_t to be computed directly from the forward-pass quantities (p_t and \mathbf{h}_t) without any additional backpropagation. Consequently, STAG captures fine-grained adaptation behavior at each time step with negligible computational overhead, providing the vector required for subsequent structural alignment.

Structural Gradient Alignment The final objective of STAG is to rectify the instantaneous adaptation direction by aligning it with the model’s intrinsic structural knowledge. Given the online gradient \mathbf{g}_t and the corresponding structural anchor $\mathbf{a}_{\hat{y}_t}$, we define the alignment loss $\mathcal{L}_{\text{STAG}}$ as the negative cosine similarity between the two vectors:

$$\mathcal{L}_{\text{STAG}}(\mathbf{x}_t) = -\frac{\mathbf{g}_t \cdot \mathbf{a}_{\hat{y}_t}}{\|\mathbf{g}_t\| \|\mathbf{a}_{\hat{y}_t}\| + \epsilon}, \quad (7)$$

where ϵ is a small constant for numerical stability.

For a mini-batch \mathcal{B}_t arriving at step t , the batch-wise alignment loss is the empirical mean over the samples:

$$\mathcal{L}_{\text{STAG}}(\mathcal{B}_t) = \frac{1}{|\mathcal{B}_t|} \sum_{\mathbf{x} \in \mathcal{B}_t} \mathcal{L}_{\text{STAG}}(\mathbf{x}). \quad (8)$$

The final objective to be minimized at step t is formulated as a weighted combination of a baseline TTA loss and the proposed $\mathcal{L}_{\text{STAG}}$:

$$\mathcal{L}_{\text{total}} = \mathcal{L}_{\text{base}}(\mathcal{B}_t) + \beta_t \mathcal{L}_{\text{STAG}}(\mathcal{B}_t), \quad (9)$$

where $\mathcal{L}_{\text{base}}$ denotes an arbitrary unsupervised objective used in standard TTA frameworks (e.g., Shannon entropy in

TENT (Wang et al., 2021) or importance-weighted entropy in EATA (Niu et al., 2022)). Here, β_t is a dynamic balancing coefficient that follows an exponential decay:

$$\beta_{t+1} = \beta_t \cdot \exp(-1/\gamma). \quad (10)$$

This decaying strategy ensures strong structural guidance in the early stages of adaptation to prevent initial semantic drift, while gradually relaxing the constraint as the model becomes more familiar with the target domain. By framing STAG as a structural regularizer, it can be seamlessly integrated into various baseline TTA methods to enhance their architectural consistency and adaptation stability. The entire procedure is summarized in Appendix B (Algorithm 1).

3.3. Computational Complexity

Compared to standard TTA methods, the computational overhead of STAG is virtually negligible due to its analytical nature. The complexity varies slightly depending on whether the classifier weights W are updated:

- **Static Classifier:** If the classifier W remains frozen (e.g., when only *affine parameters* of the normalization layers are adapted), the structural anchors are computed only *once* offline. The online overhead is then strictly limited to vector indexing and cosine similarity calculations, adding a negligible $O(|\mathcal{B}_t| \cdot D)$ per batch.
- **Dynamic Classifier:** If W is updated during adaptation, the anchors \mathbf{a}_k are recalculated to maintain geometric consistency. However, since the sensitivity s_k is derived from a closed-form analytical solution (Eq. 4), this process requires only a single matrix multiplication WW^\top and element-wise operations.

Crucially, this recalculation is equivalent to a single ”self-forward pass” of the classifier and **does not increase the number of backward passes**. Since the cost of a full backward pass through the network parameters θ is significantly higher than a classifier-level matrix multiplication ($|\theta| \gg C^2 D$), STAG provides structural guidance with near-zero latency compared to the baseline adaptation time.

4. Experiments

In this section, we evaluate the efficacy of STAG across a diverse range of test-time adaptation scenarios, including image classification and semantic segmentation tasks, while further extending our evaluation to challenging regimes such as imbalanced label shifts, single-sample adaptation, mixed corruption streams, and long-horizon continual TTA.

4.1. Experimental Setup

Datasets We evaluate STAG on two primary tasks to assess its versatility. For image classification, we use

Table 1. Classification accuracy (%) on ImageNet-C (severity 5) under the mild scenario. For each baseline and its STAG-integrated version (+STAG), the superior performance is highlighted in **bold**. Values in parentheses indicate the absolute accuracy gain achieved by STAG.

Mild	Noise			Blur			Weather			Digital			Avg.			
	Gauss.	Shot	Impul.	Defoc.	Glass	Motion	Zoom	Snow	Frost	Fog	Brit.	Contr.	Elastic	Pixel	JPEG	
ResNet50-BN	2.2	2.9	1.8	17.9	9.8	14.8	22.5	16.9	23.3	24.4	58.9	5.4	16.9	20.6	31.7	18.0
• TENT	28.6	30.5	30.0	28.0	27.3	41.2	49.2	47.1	41.1	57.6	67.4	27.0	54.6	58.5	52.3	42.7
+STAG	30.5 _{±0.2}	32.3 _{±0.5}	32.3 _{±0.2}	30.1 _{±0.2}	29.2 _{±0.5}	44.6 _{±0.2}	50.7 _{±0.2}	49.6 _{±0.2}	43.3 _{±0.0}	58.6 _{±0.2}	67.3 _{±0.1}	31.4 _{±0.5}	56.4 _{±0.2}	59.7 _{±0.1}	53.8 _{±0.2}	44.7 _{±0.1 (+1.96)}
• EATA	34.9	36.9	35.7	33.5	33.1	47.0	52.7	51.3	45.5	59.9	67.9	44.6	57.9	60.4	54.9	47.7
+STAG	35.6 _{±0.1}	38.0 _{±0.2}	36.7 _{±0.3}	34.6 _{±0.3}	34.1 _{±0.3}	48.9 _{±0.1}	53.2 _{±0.1}	52.7 _{±0.1}	46.5 _{±0.2}	60.4 _{±0.1}	67.6 _{±0.0}	46.4 _{±0.1}	58.5 _{±0.2}	60.8 _{±0.0}	55.5 _{±0.2}	48.6 _{±0.0 (+0.89)}
• SAR	30.7	30.4	31.1	28.9	28.9	41.8	49.3	47.2	42.2	57.5	67.3	37.2	54.5	58.4	52.3	43.8
+STAG	32.9 _{±0.2}	33.7 _{±0.2}	33.4 _{±0.5}	31.3 _{±0.5}	31.4 _{±0.4}	45.3 _{±0.1}	51.1 _{±0.1}	50.2 _{±0.1}	44.1 _{±0.2}	59.0 _{±0.1}	67.7 _{±0.1}	40.8 _{±1.1}	56.7 _{±0.1}	60.1 _{±0.1}	54.2 _{±0.2}	46.1 _{±0.1 (+2.29)}
• DeYO	35.6	38.1	36.8	33.8	33.8	48.4	52.8	52.6	46.2	60.6	68.0	44.6	58.4	61.4	55.7	48.5
+STAG	35.9 _{±0.1}	38.3 _{±0.1}	37.0 _{±0.4}	34.1 _{±0.4}	34.1 _{±0.4}	49.0 _{±0.1}	53.0 _{±0.0}	53.1 _{±0.1}	46.5 _{±0.3}	60.8 _{±0.1}	67.8 _{±0.1}	44.0 _{±3.9}	58.6 _{±0.0}	61.5 _{±0.1}	55.8 _{±0.1}	48.6 _{±0.3 (+0.17)}
ResNet50-GN	18.0	19.8	17.9	19.8	11.3	21.4	24.9	40.4	47.3	33.6	69.3	36.3	18.6	28.4	52.3	30.6
• TENT	5.0	6.6	5.7	15.1	7.9	21.9	22.7	26.3	33.2	3.3	70.3	42.4	11.0	48.1	54.3	24.9
• EATA	37.5	39.9	38.8	28.3	27.2	36.7	39.1	50.9	49.4	55.2	72.0	50.1	41.8	55.7	58.1	45.4
+STAG	44.1 _{±0.3}	46.1 _{±0.3}	44.9 _{±0.3}	34.0 _{±1.4}	35.6 _{±0.6}	46.0 _{±0.3}	49.5 _{±0.2}	58.8 _{±0.2}	54.8 _{±0.2}	63.3 _{±0.5}	73.2 _{±0.0}	55.3 _{±0.1}	55.5 _{±0.4}	63.1 _{±0.1}	60.9 _{±0.1}	52.3 _{±0.1 (+6.97)}
• SAR	28.2	31.3	29.6	18.8	19.3	30.4	30.5	41.8	43.3	44.4	70.7	43.9	17.1	48.7	55.2	36.9
+STAG	39.1 _{±0.0}	42.3 _{±0.2}	40.8 _{±0.3}	17.5 _{±0.3}	23.5 _{±1.0}	36.6 _{±0.6}	39.5 _{±0.7}	51.2 _{±0.4}	48.8 _{±0.2}	52.8 _{±3.0}	73.2 _{±0.1}	49.3 _{±0.1}	1.4 _{±0.2}	55.8 _{±0.2}	56.7 _{±0.1}	41.9 _{±0.3 (+5.01)}
• DeYO	39.6	42.3	40.9	22.7	24.7	38.9	37.2	51.6	49.8	38.3	73.2	50.4	42.9	56.6	58.0	44.5
+STAG	41.4 _{±0.2}	44.2 _{±0.4}	42.7 _{±0.5}	22.9 _{±0.1}	25.5 _{±0.3}	40.1 _{±0.1}	37.8 _{±1.4}	53.6 _{±0.2}	51.3 _{±0.1}	57.8 _{±1.0}	73.5 _{±0.1}	51.4 _{±0.2}	43.0 _{±1.6}	57.9 _{±0.2}	58.4 _{±0.1}	46.8 _{±0.1 (+2.29)}
VitBase-LN	9.5	6.7	8.2	29.0	23.4	33.9	27.1	15.9	26.5	47.2	54.7	44.1	30.5	44.5	47.8	29.9
• TENT	42.1	1.3	43.0	52.3	47.7	55.2	49.9	18.7	21.6	66.3	74.7	64.7	51.8	66.6	63.9	48.0
+STAG	52.1 _{±0.0}	0.3 _{±0.1}	53.1 _{±0.1}	57.6 _{±0.1}	57.9 _{±0.2}	62.3 _{±0.1}	59.8 _{±0.2}	65.3 _{±1.1}	52.4 _{±15.1}	73.0 _{±0.2}	77.5 _{±0.0}	68.0 _{±0.2}	66.7 _{±0.1}	72.5 _{±0.1}	69.6 _{±0.1}	59.2 _{±1.1 (+11.21)}
• EATA	50.4	50.0	51.2	55.7	55.8	60.0	57.6	63.6	61.9	71.3	76.1	66.9	64.5	70.4	67.5	61.5
+STAG	54.9 _{±0.3}	55.8 _{±0.3}	55.7 _{±0.3}	58.4 _{±0.2}	59.6 _{±0.1}	64.6 _{±0.3}	63.6 _{±0.2}	68.8 _{±0.3}	67.1 _{±0.3}	73.7 _{±0.2}	77.4 _{±0.2}	68.2 _{±0.1}	69.7 _{±0.2}	73.1 _{±0.3}	70.0 _{±0.2}	65.4 _{±0.2 (+3.85)}
• SAR	43.8	33.7	44.8	52.9	50.0	55.9	51.2	57.3	55.6	66.3	74.7	64.4	55.1	66.6	63.9	55.8
+STAG	54.0 _{±0.2}	53.3 _{±2.2}	53.1 _{±3.3}	58.2 _{±0.1}	59.3 _{±0.2}	63.5 _{±0.1}	62.0 _{±0.1}	67.5 _{±0.2}	66.0 _{±0.1}	73.6 _{±0.1}	77.8 _{±0.1}	67.8 _{±0.4}	68.7 _{±0.2}	73.2 _{±0.1}	70.2 _{±0.0}	64.5 _{±0.3 (+8.79)}
• DeYO	53.3	52.1	54.2	58.3	58.7	63.1	51.6	67.3	66.1	73.2	78.1	68.0	68.0	73.2	70.1	63.7
+STAG	56.1 _{±0.3}	57.4 _{±0.2}	56.5 _{±0.5}	58.9 _{±0.2}	60.3 _{±0.1}	65.8 _{±0.0}	65.4 _{±0.1}	69.1 _{±0.5}	66.7 _{±0.6}	73.6 _{±0.6}	77.6 _{±0.1}	67.2 _{±0.3}	71.1 _{±0.0}	73.8 _{±0.2}	70.0 _{±0.6}	66.0 _{±0.1 (+2.26)}

ImageNet-C and CIFAR-10/100-C (Hendrycks & Dietterich, 2019), widely used benchmarks for evaluating model robustness and test-time adaptation. Both datasets consist of 15 corruption types with 5 severity levels. For semantic segmentation, we use the Cityscapes-to-ACDC benchmark, where Cityscapes (Cordts et al., 2016) is the source domain and the Adverse Conditions Dataset with Correspondences (ACDC) (Sakaridis et al., 2021) is the target domain with four weather corruptions: Fog, Night, Rain, and Snow.

Architectures For CIFAR-10/100-C, we use WideResNet-28/40 (Zagoruyko & Komodakis, 2016), respectively. For ImageNet-C, we evaluate ResNet50-BN, ResNet50-GN, and VitBase-LN, using models from `torchvision` or `timm` (Wightman, 2019). For segmentation, we adopt a pretrained Segformer-B5 (Xie et al., 2021).

Baselines We compare against representative TTA methods: **Source** (no adaptation), **TENT** (Wang et al., 2021) (entropy minimization), **EATA** (Niu et al., 2022) (stability regularization with re-weighting), **SAR** (Niu et al., 2023) (sharpness-aware updates with noisy-sample filtering), and **DeYO** (Lee et al., 2024) (confidence-based filtering via PLPD). For continual TTA, we additionally consider **BN Adapt** (Nado et al., 2020), **CoTTA** (Wang et al., 2022), and **EcoTTA** (Song et al., 2023) (partition factor $K \in \{4, 5\}$).

Implementation Details We follow each baseline’s original optimization protocol for fair comparison. STAG uses two hyper-parameters, β_0 and γ , selected using only a single corruption type (the first corruption in our evaluation order)

and then fix them for all remaining corruption types. The specific hyperparameter configurations for each experimental setting are detailed in Appendix B (Table 10).

4.2. Main Results on Image Classification

The **mild scenario** is a standard test-time adaptation setting with a large batch size ($B = 64$) and a stationary distribution, serving as a benchmark before more extreme dynamic shifts. Table 1 summarizes the classification accuracy on ImageNet-C (severity 5). We observe that STAG improves all four baselines across architectures. In **ResNet50-BN**, STAG yields an average gain of up to **+2.29%** points. The gains are larger on non-BN models: for **ResNet50-GN**, adding STAG to EATA improves accuracy by **+6.97%** to 52.3%, and for **VitBase-LN**, TENT+STAG achieves the largest boost of **+11.21%** points (48.0% \rightarrow 59.2%). These results suggest that STAG regularizes adaptation across diverse architectures. We further analyze stability using accuracy running curves under Gaussian noise. As shown in Figure 3, STAG (dashed) yields higher accuracy and more stable convergence than the original baselines (solid), with faster initial improvement and a better steady state. Detailed per-condition curves are provided in Figure 8.

t-SNE Visualization To qualitatively investigate the impact of STAG on the model’s internal representations, we visualize the feature space using t-SNE (Van der Maaten & Hinton, 2008). Figure 4 illustrates the feature distributions for VitBase-LN on the ImageNet-C Frost dataset at

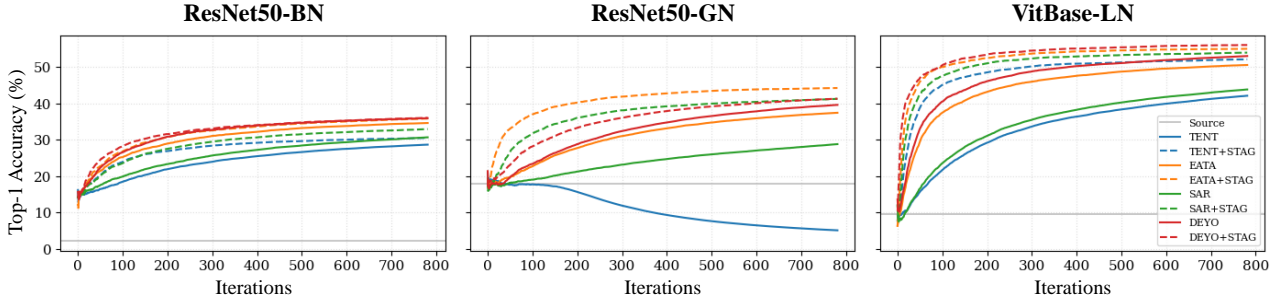


Figure 3. Top-1 accuracy running curves across three different architectures on ImageNet-C Gaussian noise (severity 5)

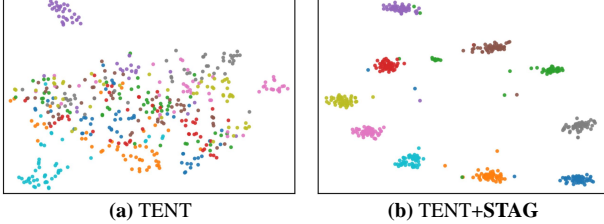


Figure 4. The t-SNE visualization of the feature space on ImageNet-C Frost (severity 5)

severity level 5. As shown in Figure 4(a), the feature space of the baseline **TENT** exhibits heavily overlapped clusters, indicating a loss of discriminative power under severe distortions. In contrast, **TENT+STAG** (Figure 4(b)) yields significantly tighter and better-separated clusters. This visualization confirms that STAG effectively regularizes the adaptation process, maintaining the semantic structure of the feature space even under significant distribution shifts.

4.3. Results in Dynamic Scenario

We evaluate STAG under three realistic dynamic settings proposed by (Niu et al., 2023), where the test stream is *non-stationary*.

Online Imbalanced Label Distribution Shifts This setting simulates *class-prior shift* at test time: the incoming stream is organized into consecutive phases in which the label distribution becomes highly skewed toward a subset of classes, and the dominant classes remain overrepresented for a while before the stream shifts again. Such imbalance can amplify confirmation bias in pseudo-labeling and destabilize entropy-based updates. As summarized in Table 3, STAG improves robustness under these imbalanced priors by stabilizing the adaptation signal, yielding average gains of up to **7.33%** for TENT (ResNet50-GN) and **5.79%** for SAR (VitBase-LN).

Batch Size 1 (Single-sample Adaptation) Single-sample adaptation ($B=1$) is challenging online regime, where the model updates after each test example with no batch statistics and minimal averaging. This setting is particularly prone

Table 2. Classification accuracy (%) on ImageNet-C (severity 5) under the mixed distribution shift.

Model	ResNet50-GN			VitBase-LN		
	Original	+ STAG	Gain	Original	+ STAG	Gain
Source	30.6	-	-	29.9	-	-
TENT	13.3	-	-	15.8	-	-
EATA	38.0	39.4 ± 0.3	+1.5	56.5	57.8 ± 0.6	+1.3
SAR	38.3	38.9 ± 0.5	+0.6	57.1	59.8 ± 0.1	+2.7
DeYO	38.0	38.8 ± 1.6	+0.8	58.9	59.7 ± 0.4	+0.8

to noisy gradients and error accumulation, often causing abrupt performance collapse for unstable objectives. As shown in Table 3, STAG acts as a strong regularizer in this extreme regime, providing substantial absolute improvements of **10.68%** points for EATA on ResNet50-GN and **11.71%** points on VitBase-LN.

Mixed Distribution Shifts This setting evaluates adaptation on a mixed-corruption test set, constructed by combining samples from all 15 corruption types. Rather than adapting to a single fixed corruption, the model must handle heterogeneous corruptions within the same evaluation stream, which makes the pseudo-labels and entropy signal more variable. Table 2 reports the results over a mixture of 15 corruption types. STAG consistently improves performance in this non-stationary stream, achieving a **1.5%** points gain for EATA on ResNet50-GN and a **2.7%** points gain for SAR on VitBase-LN.

4.4. Results in Continual Test-Time Adaptation

Continual TTA considers long-horizon online adaptation on a *non-stationary* target stream without access to source data, requiring robustness to error accumulation and catastrophic forgetting. For classification, models pre-trained on clean CIFAR-10 or CIFAR-100 are continually adapted online to sequentially encountered corruption types. All results are reported at the highest corruption severity (level 5). For segmentation, following (Wang et al., 2022), we evaluate Cityscapes-to-ACDC under a cyclic weather stream that repeats Fog \rightarrow Night \rightarrow Rain \rightarrow Snow for ten rounds (40 stages), emphasizing long-term stability through repeated

Table 3. Classification accuracy (%) on ImageNet-C (severity 5) under the imbalanced label shifts (imbalance ratio = ∞) or the batch size 1.

Label Shifts	Noise			Blur			Weather			Digital			Avg.			
	Gauss.	Shot	Impul.	Defoc.	Glass	Motion	Zoom	Snow	Frost	Fog	Brit.	Contr.	Elastic	Pixel	JPEG	
ResNet50-GN	18.0	19.8	17.9	19.8	11.3	21.4	24.9	40.4	47.3	33.6	69.3	36.3	18.6	28.4	52.3	30.6
• TENT	2.6	3.2	2.9	13.5	5.4	18.8	16.7	15.8	21.1	1.8	70.4	42.1	6.3	49.4	53.6	21.6
• EATA	26.9	31.0	26.0	18.2	17.8	23.7	26.8	34.4	32.4	41.8	66.9	33.7	26.0	41.7	41.6	32.6
+STAG	29.6 _{±0.3}	30.8 _{±1.9}	30.1 _{±0.7}	20.2 _{±4.6}	21.0 _{±1.8}	33.1 _{±1.6}	35.4 _{±0.9}	46.7 _{±0.7}	43.9 _{±1.6}	50.4 _{±2.5}	68.9 _{±0.7}	42.3 _{±1.0}	39.6 _{±1.6}	53.8 _{±0.4}	53.5 _{±1.4}	39.9 _{±0.4} (+7.33)
• SAR	33.8	36.5	34.9	19.3	20.2	33.4	29.2	23.7	45.0	34.6	7.9	46.7	6.9	52.1	56.3	36.3
+STAG	37.8 _{±2.2}	40.4 _{±1.8}	39.3 _{±1.0}	18.7 _{±0.8}	16.1 _{±0.7}	35.2 _{±2.0}	37.8 _{±0.5}	40.4 _{±0.9}	47.9 _{±0.9}	18.8 _{±30.9}	73.2 _{±0.1}	49.0 _{±0.2}	1.0 _{±0.2}	55.1 _{±0.1}	56.9 _{±0.1}	37.8 _{±2.7} (+1.53)
• DeYO	40.0	44.1	42.6	22.0	23.5	41.1	8.2	52.2	51.2	19.5	73.2	52.7	37.7	59.4	59.1	41.8
+STAG	42.6 _{±1.2}	44.8 _{±0.3}	43.5 _{±0.8}	21.4 _{±1.2}	7.7 _{±11.9}	41.7 _{±0.6}	14.3 _{±16.0}	54.4 _{±1.0}	52.5 _{±0.3}	20.4 _{±34.1}	73.5 _{±0.1}	52.9 _{±0.3}	34.1 _{±24.1}	60.1 _{±0.4}	59.3 _{±0.2}	41.5 _{±1.8} (0.22)
VitBase-LN	9.5	6.7	8.2	29.0	23.4	33.9	27.1	15.9	26.5	47.2	54.7	44.1	30.5	44.5	47.8	29.9
• TENT	32.6	0.9	29.3	54.6	52.5	58.2	52.8	9.4	10.4	69.3	76.1	65.9	57.7	69.4	66.4	47.0
+STAG	35.8 _{±7.6}	0.6 _{±0.6}	38.8 _{±16.5}	56.3 _{±0.0}	55.7 _{±0.1}	60.2 _{±0.1}	55.8 _{±1.3}	19.1 _{±5.0}	15.4 _{±3.9}	71.5 _{±0.3}	77.1 _{±0.1}	67.1 _{±0.0}	62.5 _{±1.3}	71.2 _{±0.1}	68.4 _{±0.1}	50.4 _{±1.9} (+3.33)
• EATA	36.3	37.3	37.0	41.3	44.6	49.4	39.7	54.9	51.8	47.3	73.9	27.5	57.6	64.9	62.8	48.4
+STAG	36.9 _{±2.1}	34.7 _{±1.9}	36.6 _{±1.8}	38.9 _{±4.7}	43.8 _{±1.1}	49.0 _{±1.1}	46.1 _{±1.8}	55.5 _{±1.4}	53.2 _{±1.5}	57.9 _{±5.0}	74.0 _{±0.8}	21.9 _{±16.2}	58.9 _{±0.8}	64.8 _{±1.3}	63.6 _{±0.5}	49.1 _{±0.6} (+0.64)
• SAR	46.5	36.1	48.8	55.3	54.3	58.9	54.8	51.0	46.3	69.7	76.2	66.2	60.8	69.6	66.6	57.4
+STAG	52.7 _{±1.6}	51.4 _{±3.1}	52.9 _{±1.9}	57.8 _{±0.1}	59.1 _{±0.1}	63.3 _{±0.1}	61.4 _{±0.6}	67.6 _{±0.2}	50.9 _{±13.4}	73.7 _{±0.1}	77.9 _{±0.1}	67.4 _{±0.2}	68.5 _{±0.3}	73.4 _{±0.1}	70.0 _{±0.1}	63.2 _{±1.3} (+5.79)
• DeYO	35.8	51.7	53.4	57.7	58.8	63.7	39.0	67.9	66.2	73.1	77.9	66.6	68.9	73.6	70.3	61.6
+STAG	53.1 _{±1.2}	53.6 _{±2.6}	54.4 _{±1.6}	57.8 _{±0.1}	59.0 _{±0.2}	64.4 _{±0.2}	55.2 _{±12.7}	68.6 _{±0.1}	66.3 _{±0.1}	73.4 _{±0.2}	78.0 _{±0.0}	66.7 _{±0.2}	69.6 _{±0.1}	73.9 _{±0.1}	70.6 _{±0.2}	64.3 _{±1.2} (+2.67)
Batch Size 1	Noise			Blur			Weather			Digital			Avg.			
	Gauss.	Shot	Impul.	Defoc.	Glass	Motion	Zoom	Snow	Frost	Fog	Brit.	Contr.	Elastic	Pixel	JPEG	
ResNet50-GN	18.0	19.8	17.9	19.8	11.3	21.4	24.9	40.4	47.3	33.6	69.3	36.3	18.6	28.4	52.3	30.6
• TENT	2.3	3.1	2.7	13.2	4.7	18.0	18.7	16.2	20.8	1.4	70.3	42.2	6.0	49.3	53.7	21.5
• EATA	24.9	28.1	25.6	17.9	17.1	28.6	29.4	44.7	44.4	39.8	70.9	44.3	26.9	46.4	55.6	36.3
+STAG	38.9 _{±0.3}	42.2 _{±0.2}	40.7 _{±0.2}	17.9 _{±0.1}	27.3 _{±0.4}	39.9 _{±0.4}	43.0 _{±0.3}	55.1 _{±0.3}	51.9 _{±0.2}	58.4 _{±0.1}	73.2 _{±0.1}	51.8 _{±0.2}	47.0 _{±0.2}	58.6 _{±0.2}	59.0 _{±0.2}	47.0 _{±0.1} (+10.68)
• SAR	23.4	26.6	23.6	18.6	15.0	28.8	30.3	45.1	44.6	27.6	72.3	44.7	13.2	46.8	56.1	34.4
+STAG	43.5 _{±0.3}	46.0 _{±0.2}	44.7 _{±0.1}	12.6 _{±0.1}	10.2 _{±1.9}	41.6 _{±0.3}	46.5 _{±0.4}	59.0 _{±0.3}	54.0 _{±0.0}	51.9 _{±19.0}	73.2 _{±0.1}	52.6 _{±0.1}	6.5 _{±0.8}	61.8 _{±0.1}	58.4 _{±0.0}	44.2 _{±1.1} (+9.72)
• DeYO	37.1	40.7	39.0	21.3	23.1	37.4	37.3	51.6	49.5	3.4	73.2	50.7	41.0	56.4	58.2	41.3
+STAG	41.2 _{±0.3}	44.3 _{±0.1}	42.5 _{±0.4}	20.8 _{±0.2}	24.3 _{±0.3}	40.1 _{±0.1}	40.5 _{±0.7}	56.3 _{±0.2}	52.3 _{±0.1}	58.7 _{±0.5}	73.7 _{±0.0}	52.4 _{±0.1}	27.1 _{±15.5}	59.5 _{±0.1}	59.0 _{±0.1}	46.2 _{±1.0} (+4.86)
VitBase-LN	9.5	6.7	8.2	29.0	23.4	33.9	27.1	15.9	26.5	47.2	54.7	44.1	30.5	44.5	47.8	29.9
• TENT	42.3	1.0	43.2	52.6	48.1	55.4	50.1	16.5	18.4	66.5	74.9	64.7	52.6	66.8	64.1	47.8
+STAG	53.6 _{±0.4}	18.4 _{±31.3}	38.3 _{±28.5}	58.3 _{±0.2}	59.1 _{±0.0}	63.9 _{±0.0}	62.2 _{±0.2}	46.0 _{±38.0}	45.2 _{±36.6}	73.3 _{±0.1}	77.5 _{±0.0}	68.2 _{±0.1}	68.7 _{±0.1}	72.9 _{±0.1}	69.9 _{±0.1}	58.4 _{±5.1} (+10.55)
• EATA	32.6	27.7	33.7	44.9	40.8	47.3	42.7	39.4	43.8	62.4	67.0	62.0	47.3	60.8	59.3	47.4
+STAG	50.7 _{±1.4}	50.3 _{±1.8}	51.4 _{±1.6}	53.7 _{±0.9}	55.5 _{±1.1}	60.0 _{±1.0}	59.0 _{±1.3}	64.0 _{±1.8}	62.5 _{±1.6}	71.6 _{±0.4}	75.3 _{±0.8}	46.0 _{±34.3}	49.6 _{±29.1}	70.2 _{±0.9}	67.5 _{±0.7}	59.2 _{±2.7} (+11.71)
• SAR	40.8	36.5	41.8	53.5	50.6	57.4	52.8	58.8	54.8	67.6	75.5	65.6	58.2	68.8	65.8	56.6
+STAG	56.3 _{±0.2}	57.6 _{±0.1}	57.1 _{±0.1}	59.2 _{±0.2}	60.5 _{±0.1}	65.9 _{±0.2}	65.1 _{±1.9}	67.9 _{±1.5}	67.2 _{±0.2}	72.5 _{±0.5}	76.8 _{±0.2}	67.6 _{±0.4}	68.0 _{±1.8}	72.2 _{±1.0}	69.1 _{±0.1}	65.5 _{±0.3} (+8.95)
• DeYO	51.0	45.8	51.8	57.7	57.6	62.4	57.0	66.2	65.1	72.8	77.9	68.0	66.4	72.5	69.6	62.8
+STAG	56.2 _{±0.0}	57.6 _{±0.1}	56.9 _{±0.1}	58.9 _{±0.2}	60.3 _{±0.1}	44.9 _{±36.1}	61.5 _{±7.8}	69.2 _{±0.0}	66.9 _{±0.5}	73.4 _{±0.1}	77.0 _{±0.1}	70.5 _{±0.1}	73.4 _{±0.1}	70.4 _{±0.1}	63.1 _{±2.5} (+0.34)	

re-adaptation to previously encountered conditions.

Continual classification. Table 4 reports classification error rates (%) on CIFAR-10-C and CIFAR-100-C (severity 5). STAG consistently reduces error across diverse continual TTA baselines, yielding substantial gains for BN Adapt (**20.4**→**17.9**, **39.3**→**36.7**) and TENT (**19.0**→**17.4**, **37.2**→**35.4**), while also providing additional improvements for stronger methods such as CoTTA and EcoTTA. The error rates for each corruption type are provided in Appendix B (Tables 7 and 8). These results indicate that STAG complements existing continual objectives as a lightweight stabilizer, improving robustness without changing each method’s optimization protocol.

Continual semantic segmentation. Figure 5 compares TENT and TENT+STAG on Cityscapes-to-ACDC over ten rounds using per-weather mIoU. TENT exhibits clear forgetting, with performance progressively degrading across cycles due to accumulated drift from sequential adaptation. In contrast, TENT+STAG maintains consistently higher mIoU across repeated cycles and, in some cases, even shows performance improvements, indicating that STAG provides a structural prior that counteracts long-horizon drift in con-

Table 4. Classification error rate (%) on CIFAR-10-C (severity 5) and CIFAR-100-C (severity 5) in continual test-time adaptation tasks.

Dataset (Model)	CIFAR-10-C (WRN-28)			CIFAR-100-C (WRN-40)		
	Original	+ STAG	Gain	Original	+ STAG	Gain
Source	43.5	-	-	46.8	-	-
BN Adapt	20.4	17.9 _{±0.0}	+2.5	39.3	36.7 _{±0.0}	+2.6
TENT	19.0	17.4 _{±0.0}	+1.6	37.2	35.4 _{±0.0}	+1.8
CoTTA	16.3	16.1 _{±0.0}	+0.2	38.1	37.4 _{±0.0}	+0.7
EcoTTA (K = 4)	17.9	17.5 _{±0.0}	+0.4	36.8	36.6 _{±0.0}	+0.2
EcoTTA (K = 5)	18.0	17.6 _{±0.0}	+0.4	36.8	36.7 _{±0.0}	+0.1

tinual adaptation. Detailed results, including BN Adapt and BN Adapt+STAG, are reported in Appendix B (Table 9). Figure 6 qualitatively supports this observation, showing that TENT+STAG produces more coherent segmentation maps with fewer artifacts and better scene preservation under Fog, Night, Rain, and Snow. These results demonstrate that STAG mitigates forgetting and stabilizes continual TTA under cyclic, non-stationary shifts.

4.5. Ablation Study

Sensitivity of Hyper-parameters We analyze the sensitivity of STAG to its two key hyper-parameters: the initial balancing coefficient β_0 and the decay factor γ . Figure 7 re-

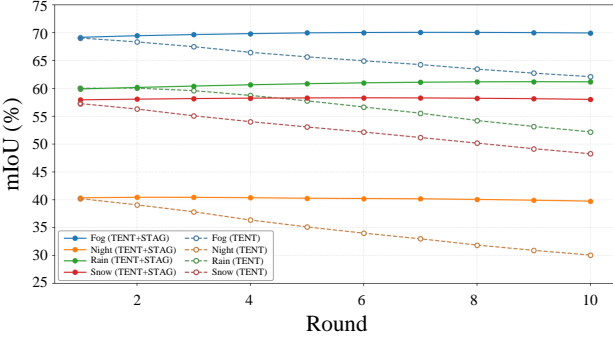


Figure 5. Semantic segmentation performance (mIoU, %) between TENT and its STAG-integrated version on the Cityscapes-to-ACDC continual test-time adaptation tasks.

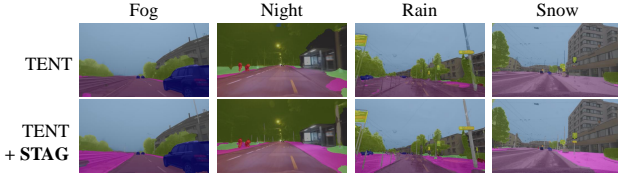


Figure 6. Semantic segmentation maps on the Cityscapes-to-ACDC continual test-time adaptation task at the 10th round.

ports Top-1 accuracy on ImageNet-C Gaussian noise (severity 5), where the x-axes in (a) and (b) are normalized by the optimal values (β^* , γ^* ; see Appendix B (Table 10)). The red dashed line indicates the normalized optimum (1.0), around which we observe a broad plateau, suggesting that STAG is robust to moderate perturbations of both hyper-parameters. Across a wide range, STAG remains above the TENT baseline and shows similar trends on ResNet50-BN and VitBase-LN. Panel (c) shows that larger β_0 and slower decay (larger γ) generally improve performance on VitBase-LN, while (d) illustrates the corresponding schedule $\beta_t/\beta_0 = \exp(-t/\gamma)$. Overall, STAG provides robust gains without requiring precise hyper-parameter tuning.

Ablation on Design Choices We conduct an ablation study on VitBase-LN under Gaussian noise to validate our design choices for structural anchor (*Diagonal* vs. *Full*) and weighting schemes (*Hard* vs. *Soft labels*). Table 5 indicates that the **Diagonal/Hard** setting performs best in most cases across the baselines. Using only diagonal gradient elements outperforms the full gradient (e.g., 52.13% vs. 49.24% for TENT), indicating that the diagonal approximation captures useful structure while mitigating noise from cross-parameter correlations. Hard pseudo-labels also outperform soft labels, which can become ambiguous under heavy noise. With this design, STAG improves TENT and SAR by **+9.96%** points and **+9.81%** points, respectively.

Computational Efficiency Empirically, comparing forward/backward cost, runtime, and memory usage shows that STAG introduces little to no additional overhead across base-

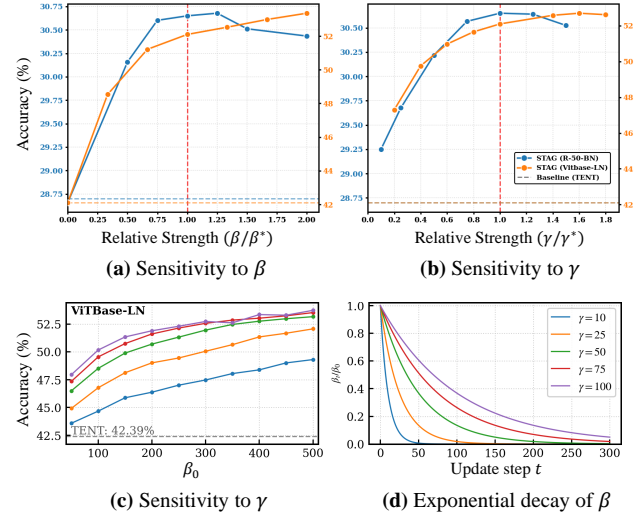


Figure 7. Hyper-parameter sensitivity analysis of STAG on ImageNet-C Gaussian Noise (Severity 5).

Table 5. Ablation study on method design using VitBase-LN on ImageNet-C Gaussian Noise (Severity 5).

Design Variant	TENT	EATA	SAR	DeYO
Baseline (No STAG)	42.17	51.07	44.06	53.11
Full / Soft	29.80	55.08	52.90	50.32
Full / Hard	49.24	52.17	47.92	51.86
Diagonal / Soft	52.92	54.79	52.24	48.43
Diagonal / Hard (Ours)	52.13	55.26	53.87	55.88

lines. This is because STAG provides structural guidance in closed form, without requiring extra backpropagation beyond the underlying baseline. Detailed statistics are reported in Appendix B (Table 6).

5. Conclusion

We presented **STAG** (Structural Test-time Alignment of Gradients), a lightweight, **plug-and-play** regularizer for online test-time adaptation under extreme information scarcity. STAG exploits an always-available structural signal—the classifier’s intrinsic geometry—by deriving class-wise structural anchors via self-structural entropy and aligning predicted-class entropy gradients to these anchors during adaptation. Thanks to its analytical closed-form formulation, STAG introduces **near-zero** memory and latency overhead and requires no additional backpropagation beyond the underlying baseline, making it practical for real-time deployment. Extensive experiments across corrupted image classification and continual semantic segmentation show that STAG consistently strengthens a wide range of TTA baselines across both CNN and Transformer architectures, while improving robustness in challenging *in-the-wild* set-

tings such as single-sample adaptation, imbalanced label shifts, and long-horizon continual adaptation. Future work includes extending structural alignment to richer heads and broader prediction settings, and developing deeper theoretical characterizations of when and why classifier geometry provides reliable guidance for test-time learning.

Impact Statement

This paper proposes a lightweight, plug-and-play regularizer for test-time adaptation that improves robustness to distribution shift without additional supervision or extra backpropagation. Its main positive impact is more reliable deployment of vision models under real-world corruptions (e.g., adverse weather), reducing performance degradation in practice. Potential risks are consistent with adaptive systems in general: online updates can still fail under unexpected out-of-distribution inputs or accumulate errors over long horizons, which may be problematic in safety-critical settings. We mitigate these concerns by evaluating across diverse shifts, architectures, and challenging continual regimes, and we recommend monitoring and conservative deployment when used in high-stakes applications.

References

Cordts, M., Omran, M., Ramos, S., Rehfeld, T., Enzweiler, M., Benenson, R., Franke, U., Roth, S., and Schiele, B. The cityscapes dataset for semantic urban scene understanding. In *Proceedings of the IEEE conference on computer vision and pattern recognition*, pp. 3213–3223, 2016.

Csurka, G. Domain adaptation for visual applications: A comprehensive survey. *arXiv preprint arXiv:1702.05374*, 2017.

Ganin, Y. and Lempitsky, V. Unsupervised domain adaptation by backpropagation. In *International conference on machine learning*, pp. 1180–1189. PMLR, 2015.

Hendrycks, D. and Dietterich, T. Benchmarking neural network robustness to common corruptions and perturbations. In *International Conference on Learning Representations*, 2019.

Hwang, U., Lee, J., Shin, J., and Yoon, S. SF(DA)²: Source-free domain adaptation through the lens of data augmentation. In *International Conference on Learning Representations*, 2024.

Krizhevsky, A., Sutskever, I., and Hinton, G. E. Imagenet classification with deep convolutional neural networks. *Communications of the ACM*, 60(6):84–90, 2017.

Lee, J., Jung, D., Yim, J., and Yoon, S. Confidence score for source-free unsupervised domain adaptation. In *International Conference on Machine Learning*, pp. 12365–12377. PMLR, 2022.

Lee, J., Jung, D., Lee, S., Park, J., Shin, J., Hwang, U., and Yoon, S. Entropy is not enough for test-time adaptation: From the perspective of disentangled factors. In *International Conference on Learning Representations*, 2024.

Liang, J., Hu, D., and Feng, J. Do we really need to access the source data? source hypothesis transfer for unsupervised domain adaptation. In *International Conference on Machine Learning*, pp. 6028–6039. PMLR, 2020.

Muandet, K., Balduzzi, D., and Schölkopf, B. Domain generalization via invariant feature representation. In *International conference on machine learning*, pp. 10–18. PMLR, 2013.

Nado, Z., Padhy, S., Sculley, D., D’Amour, A., Lakshminarayanan, B., and Snoek, J. Evaluating prediction-time batch normalization for robustness under covariate shift. *arXiv preprint arXiv:2006.10963*, 2020.

Niu, S., Wu, J., Zhang, Y., Chen, Y., Zheng, S., Zhao, P., and Tan, M. Efficient test-time model adaptation without forgetting. In *International conference on machine learning*, pp. 16888–16905. PMLR, 2022.

Niu, S., Wu, J., Zhang, Y., Wen, Z., Chen, Y., Zhao, P., and Tan, M. Towards stable test-time adaptation in dynamic wild world. In *International Conference on Learning Representations*, 2023.

Sakaridis, C., Dai, D., and Van Gool, L. Acdc: The adverse conditions dataset with correspondences for semantic driving scene understanding. In *Proceedings of the IEEE/CVF international conference on computer vision*, pp. 10765–10775, 2021.

Schneider, S., Rusak, E., Eck, L., Bringmann, O., Brendel, W., and Bethge, M. Improving robustness against common corruptions by covariate shift adaptation. *Advances in Neural Information Processing Systems*, 33: 11539–11551, 2020.

Song, J., Lee, J., Kweon, I. S., and Choi, S. Ecotta: Memory-efficient continual test-time adaptation via self-distilled regularization. In *Proceedings of the IEEE/CVF Conference on Computer Vision and Pattern Recognition*, pp. 11920–11929, 2023.

Van der Maaten, L. and Hinton, G. Visualizing data using t-sne. *Journal of machine learning research*, 9(11), 2008.

Wang, D., Shelhamer, E., Liu, S., Olshausen, B., and Darrell, T. Tent: Fully test-time adaptation by entropy minimization. In *International Conference on Learning Representations*, 2021.

Wang, Q., Fink, O., Van Gool, L., and Dai, D. Continual test-time domain adaptation. In *Proceedings of the IEEE/CVF Conference on Computer Vision and Pattern Recognition*, pp. 7201–7211, 2022.

Wightman, R. Pytorch image models. <https://github.com/rwightman/pytorch-image-models>, 2019.

Xie, E., Wang, W., Yu, Z., Anandkumar, A., Alvarez, J. M., and Luo, P. Segformer: Simple and efficient design for semantic segmentation with transformers. *Advances in neural information processing systems*, 34:12077–12090, 2021.

Zagoruyko, S. and Komodakis, N. Wide residual networks. In *British Machine Vision Conference*, 2016.

A. Analytical Derivation and Implementation-Consistent Formulation

This appendix provides an analytical derivation of the Shannon entropy gradient used in our method and clarifies the exact quantities employed in 3.2 (Anchor and Sample-wise Gradient Extraction). All logarithms are natural.

A.1. Setup and Notation

Let $\mathbf{h} = f_\phi(\mathbf{x}) \in \mathbb{R}^D$ be the feature representation of an input \mathbf{x} . The logit z_i for class i is

$$z_i = \mathbf{w}_i^\top \mathbf{h} + b_i, \quad (11)$$

and the predictive distribution is $p_i = \sigma(\mathbf{z})_i$ via softmax:

$$p_i = \frac{\exp(z_i)}{\sum_{j=1}^c \exp(z_j)}. \quad (12)$$

The Shannon entropy loss is

$$\mathcal{L}_{\text{ent}}(\mathbf{x}) = H(\mathbf{p}) = - \sum_{i=1}^c p_i \ln p_i. \quad (13)$$

A.2. Entropy Gradient with Respect to Logits

Step 1: Softmax Jacobian. The derivative of p_i with respect to z_j is

$$\frac{\partial p_i}{\partial z_j} = p_i (\delta_{ij} - p_j), \quad (14)$$

where δ_{ij} is the Kronecker delta.

Step 2: Entropy derivative with respect to probabilities.

$$\frac{\partial H}{\partial p_i} = -(\ln p_i + 1). \quad (15)$$

Step 3: Chain rule to logits.

$$\begin{aligned} \frac{\partial H}{\partial z_j} &= \sum_{i=1}^c \frac{\partial H}{\partial p_i} \frac{\partial p_i}{\partial z_j} = - \sum_{i=1}^c (\ln p_i + 1) p_i (\delta_{ij} - p_j) \\ &= -(\ln p_j + 1) p_j + p_j \sum_{i=1}^c (\ln p_i + 1) p_i \\ &= -(\ln p_j + 1) p_j + p_j \left(\sum_{i=1}^c p_i \ln p_i + \sum_{i=1}^c p_i \right) \\ &= -p_j \ln p_j - p_j + p_j (-H(\mathbf{p}) + 1) \\ &= -p_j (\ln p_j + H(\mathbf{p})). \end{aligned} \quad (16)$$

A.3. Entropy Gradient with Respect to Classifier Weights (Sample-wise Gradient Extraction)

Given an input \mathbf{x} with feature $\mathbf{h} = f_\phi(\mathbf{x}) \in \mathbb{R}^D$, we compute the *logit-level sensitivity* s for class k as the derivative of the entropy with respect to the k -th logit:

$$s \triangleq \frac{\partial H(\mathbf{p})}{\partial z_k} = -p_k (\ln p_k + H(\mathbf{p})). \quad (17)$$

The resulting entropy gradient with respect to the class weight \mathbf{w}_k is then $\nabla_{\mathbf{w}_k} \mathcal{L}_{\text{ent}}(\mathbf{x}) = s \cdot \mathbf{h}$.

For a test sample \mathbf{x}_t with feature \mathbf{h}_t and pseudo-label $\hat{y}_t = \arg \max_k p_{t,k}$, we define the sample-wise direction in the weight geometry as:

$$\mathbf{g}_t \triangleq s_t \cdot \mathbf{h}_t, \quad \text{where} \quad s_t = -p_{t,\hat{y}_t} (\ln p_{t,\hat{y}_t} + H(\mathbf{p}_t)). \quad (18)$$

This s_t captures the instantaneous sensitivity of the model's prediction at the logit level for each test instance.

A.4. Self-Structural Entropy and Diagonal Structural Sensitivity (Anchor Extraction)

This section defines the self-structural quantities used for anchor extraction. From the classifier weights $W = [\mathbf{w}_1; \dots; \mathbf{w}_c] \in \mathbb{R}^{c \times D}$, we construct the self-structural similarity logits

$$Z \in \mathbb{R}^{c \times c}, \quad Z_{kj} = \mathbf{w}_j^\top \mathbf{w}_k + b_j, \quad (19)$$

and apply row-wise softmax to obtain $p_{kj} = \text{softmax}(Z_k)_j$. The self-structural entropy for each row k is

$$H_k \triangleq - \sum_{j=1}^c p_{kj} \ln p_{kj}. \quad (20)$$

By Eq. (16), the analytical derivative of H_k with respect to the self-structural logits is

$$\frac{\partial H_k}{\partial Z_{kj}} = -p_{kj} (\ln p_{kj} + H_k). \quad (21)$$

To define the anchor as the direction that minimizes structural ambiguity, we utilize the diagonal component of the entropy gradient (Eq. 16) as the scalar *structural sensitivity* s_k :

$$s_k \triangleq -p_{kk} (\ln p_{kk} + H_k). \quad (22)$$

Using this sensitivity, the structural anchor for class k is formulated as:

$$\mathbf{a}_k = s_k \mathbf{w}_k. \quad (23)$$

By isolating this diagonal component, we focus on the self-referential descent direction of each class, effectively filtering out gradient interference from unrelated class weights while maintaining high computational efficiency.

B. Additional Results

Table 6. Efficiency comparison of TTA methods on a single Nvidia A40 GPU, processing 50,000 images.

Method	Forward	Backward	Time (s)	Memory (MB)
Source	50,000	N/A	54.57	772.5
TENT	50,000	50,000	116.00	5,506.7
+STAG	50,000	50,000	116.25	5,514.0
DeYO	84,188	25,961	151.23	5,956.8
+STAG	85,227	26,811	156.26	5,965.8

Algorithm 1: STAG Online Adaptation

Require: Pre-trained f_ϕ , classifier weights $\{\mathbf{w}_k\}_{k=1}^c$, β_0 , decay γ , baseline loss $\mathcal{L}_{\text{base}}$
Ensure: Adapted parameters θ_{adapt}

- 1: **{Phase 1: Structural Anchor Derivation}**
- 2: Precompute structural anchors $\{\mathbf{a}_k\}_{k=1}^c$ using Eq. 4
- 3: **{Phase 2: Online Gradient Alignment}**
- 4: **for** each time step $t = 0, 1, \dots$ **do**
- 5: Receive mini-batch \mathcal{B}_t and perform forward pass
- 6: Extract online gradients $\{\mathbf{g}(\mathbf{x})\}_{\mathbf{x} \in \mathcal{B}_t}$ via Eq. 6
- 7: Compute alignment loss $\mathcal{L}_{\text{STAG}}(\mathcal{B}_t)$ via Eq. 8
- 8: Update θ_{adapt} by minimizing $\mathcal{L}_{\text{total}}$ (Eq. 9)
- 9: $\beta_{t+1} \leftarrow \beta_t \cdot \exp(-1/\gamma)$ {Adaptive decay, Eq. 10}
- 10: **end for**

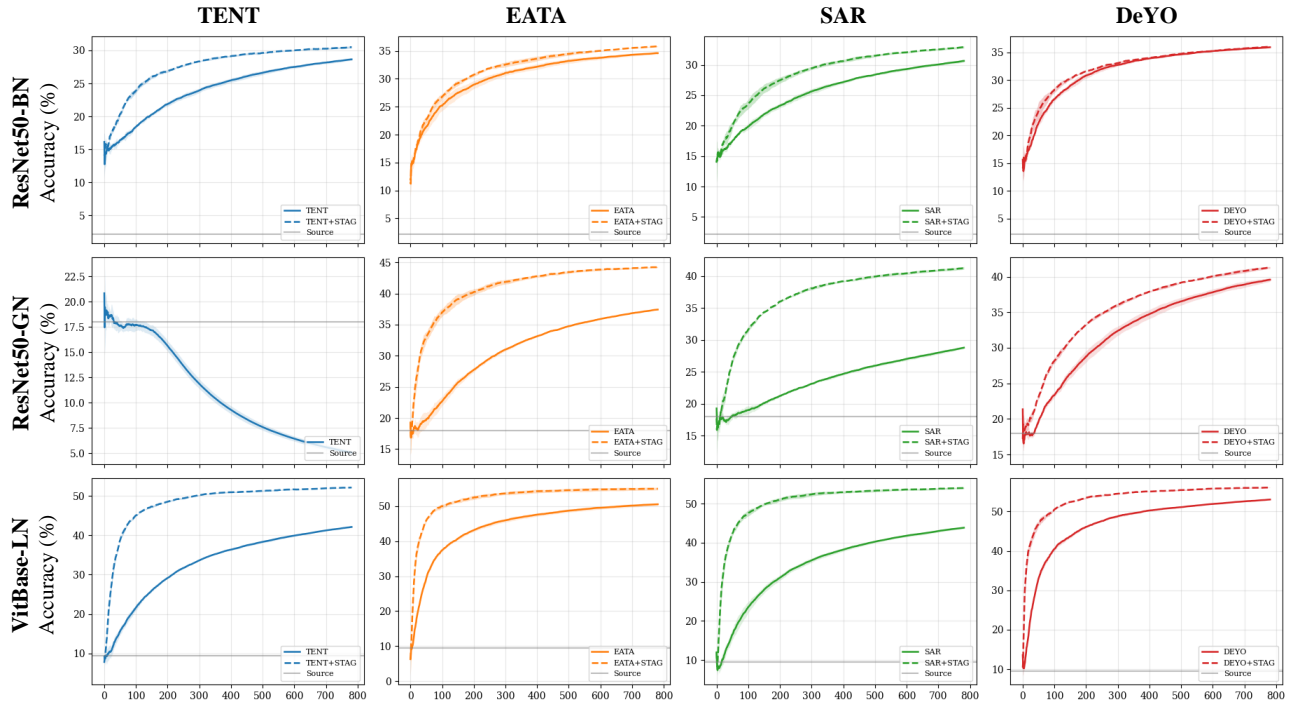


Figure 8. Detailed accuracy running curves for all architecture and baseline combinations on ImageNet-C Gaussian noise (severity 5). Each row represents a different model architecture, and each column denotes a specific adaptation baseline.

Table 7. Classification error rate (%) on CIFAR-10-C in continual test-time adaptation task. All results are evaluated on the WideResNet-28 architecture with the largest corruption severity level 5. For each baseline and its STAG-integrated version (+STAG), the superior performance is highlighted in **bold**. In cases where results are tied at the first decimal place, boldface is determined by comparing the remaining decimal digits. Values in parentheses indicate the absolute gain achieved by STAG.

Time	t	Gauss.	Shot	Impul.	Defoc.	Glass	Motion	Zoom	Snow	Frost	Fog	Brit.	Contr.	Elastic	Pixel	JPEG	Avg.
Method																	
Source		72.3	65.7	72.9	47.0	54.3	34.8	42.0	25.1	41.3	26.0	9.3	46.7	26.6	58.5	30.3	43.5
BN Adapt		28.1	26.1	36.3	12.8	35.3	14.2	12.1	17.3	17.4	15.2	8.4	12.7	23.8	19.6	27.3	20.4
+STAG		23.1\pm0.0	19.1\pm0.0	28.5\pm0.0	12.5\pm0.0	30.8\pm0.0	13.7\pm0.0	11.7\pm0.0	16.1\pm0.0	15.6\pm0.0	14.9\pm0.0	8.7\pm0.0	13.6\pm0.0	21.5\pm0.0	17.1\pm0.0	21.9\pm0.0	17.9\pm0.0 (2.5)
TENT		24.8	20.5	28.6	14.5	31.4	15.8	13.3	17.3	16.9	16.8	10.0	13.0	21.8	17.5	22.6	19.0
+STAG		23.2\pm0.0	19.5\pm0.0	28.5\pm0.0	12.3\pm0.0	30.2\pm0.0	13.8\pm0.0	11.3\pm0.0	16.0\pm0.0	15.5\pm0.0	14.6\pm0.0	8.2\pm0.0	12.0\pm0.1	20.5\pm0.0	15.2\pm0.1	20.6\pm0.0	17.4\pm0.0 (1.6)
CoTTA		24.5	22.0	26.5	11.8	27.8	12.4	10.3	14.9	14.1	12.5	7.6	10.7	18.3	13.5	17.7	16.3
+STAG		24.1\pm0.0	21.5\pm0.1	25.8\pm0.1	11.8\pm0.1	27.0\pm0.1	12.3\pm0.0	10.7\pm0.1	14.7\pm0.1	14.1\pm0.0	12.7\pm0.0	7.6\pm0.1	10.5\pm0.0	18.3\pm0.0	13.5\pm0.3	17.5\pm0.0	16.1\pm0.0 (0.2)
EcoTTA (K = 4)		25.6	20.9	28.1	11.6	31.1	14.3	11.8	16.8	15.4	14.0	8.6	12.9	20.2	16.2	20.8	17.9
+STAG		22.5\pm0.0	19.3\pm0.1	26.2\pm0.0	12.5\pm0.0	29.9\pm0.0	14.4\pm0.0	12.0\pm0.0	16.8\pm0.0	15.5\pm0.0	14.3\pm0.0	9.1\pm0.0	13.5\pm0.0	20.2\pm0.0	16.3\pm0.1	20.3\pm0.0	17.5\pm0.0 (0.4)
EcoTTA (K = 5)		25.9	21.1	28.6	11.5	31.7	14.2	11.5	16.9	15.2	13.6	9.0	13.0	20.2	16.3	20.8	18.0
+STAG		22.7\pm0.0	19.7\pm0.0	27.4\pm0.0	11.6\pm0.0	30.6\pm0.0	14.5\pm0.0	11.5\pm0.0	16.7\pm0.1	15.7\pm0.0	14.1\pm0.0	9.1\pm0.0	13.1\pm0.0	20.2\pm0.1	16.4\pm0.1	20.3\pm0.0	17.6\pm0.0 (0.4)

Table 8. Classification error rate (%) on CIFAR-100-C in continual test-time adaptation task. All results are evaluated on the WideResNet-40 architecture with the largest corruption severity level 5. For each baseline and its STAG-integrated version (+STAG), the superior performance is highlighted in **bold**. In cases where results are tied at the first decimal place, boldface is determined by comparing the remaining decimal digits. Values in parentheses indicate the absolute gain achieved by STAG.

Time	t	Gauss.	Shot	Impul.	Defoc.	Glass	Motion	Zoom	Snow	Frost	Fog	Brit.	Contr.	Elastic	Pixel	JPEG	Avg.
Method																	
Source		65.7	60.1	59.1	32.1	51.0	33.6	32.4	41.4	45.2	51.4	31.6	55.5	40.3	59.7	42.4	46.8
BN Adapt		44.3	44.0	47.3	32.1	45.9	32.8	33.0	38.3	37.9	45.4	29.9	36.5	40.6	36.7	44.1	39.3
+STAG		39.9\pm0.0	38.2\pm0.0	42.2\pm0.0	31.2\pm0.1	43.0\pm0.1	32.7\pm0.1	31.5\pm0.1	36.1\pm0.0	35.5\pm0.0	42.5\pm0.0	29.2\pm0.0	36.2\pm0.0	38.1\pm0.1	34.3\pm0.1	40.3\pm0.0	36.7\pm0.0 (2.6)
TENT		40.0	37.2	40.6	31.8	42.0	33.2	31.2	36.8	36.4	40.6	32.1	35.6	40.6	35.7	44.0	37.2
+STAG		40.9 \pm 0.0	38.8 \pm 0.0	42.2 \pm 0.0	30.1\pm0.0	42.3 \pm 0.0	31.0\pm0.0	29.8\pm0.0	34.7\pm0.0	33.9\pm0.0	39.3\pm0.0	28.0\pm0.0	31.7\pm0.0	36.6\pm0.0	31.2\pm0.0	40.7\pm0.0	35.4\pm0.0 (1.8)
CoTTA		43.5	41.6	43.7	32.2	43.6	32.7	32.2	38.6	37.5	46.0	28.9	38.0	39.3	33.9	39.3	38.1
+STAG		43.3\pm0.0	41.2\pm0.0	42.5\pm0.1	31.7\pm0.1	42.4\pm0.1	32.5\pm0.2	31.6\pm0.0	38.0\pm0.2	36.7\pm0.1	44.9\pm0.1	28.9\pm0.1	37.2\pm0.1	38.3\pm0.0	33.5\pm0.1	38.5\pm0.0	37.4\pm0.0 (0.7)
EcoTTA (K = 4)		43.5	40.3	44.7	31.5	43.8	32.2	31.1	35.8	35.0	40.0	28.4	34.5	37.6	32.5	40.8	36.8
+STAG		41.8\pm0.1	39.2\pm0.1	43.9\pm0.0	31.6 \pm 0.0	43.7\pm0.1	32.4\pm0.0	31.0\pm0.0	35.9\pm0.0	35.1\pm0.0	40.3\pm0.1	28.6\pm0.1	35.0\pm0.1	37.5\pm0.1	32.5\pm0.1	40.6\pm0.0	36.6\pm0.0 (0.2)
EcoTTA (K = 5)		44.5	40.9	44.5	31.1	43.7	32.1	31.1	35.9	34.7	39.9	28.4	34.3	37.6	32.4	40.5	36.8
+STAG		43.0\pm0.1	40.1\pm0.1	44.3\pm0.1	31.4 \pm 0.1	43.5\pm0.0	32.2\pm0.1	31.1\pm0.0	35.9\pm0.1	34.7\pm0.1	40.0\pm0.1	28.4\pm0.1	34.4\pm0.1	37.8\pm0.0	32.4\pm0.1	40.5\pm0.0	36.7\pm0.0 (0.1)

Table 9. Semantic segmentation results (mIoU in %) on the Cityscapes-to-ACDC continual test-time adaptation task. All results are evaluated on the Segformer-B5 architecture. For each baseline and its STAG-integrated version (+STAG), the superior performance is highlighted in **bold**. Values in parentheses indicate the absolute gain achieved by STAG.

Condition	t	Fog	Night	Rain	Snow	cont.																
Round	1	69.1	40.3	59.7	57.8	69.1	40.3	59.7	57.8	69.1	40.3	59.7	57.8	69.1	40.3	59.7	57.8	cont.				
Source		61.7	37.7	54.4	52.6	61.7	37.7	54.4	52.6	61.7	37.7	54.4	52.6	61.7	37.7	54.4	52.6	cont.				
BN Adapt		62.9\pm0.3	38.7\pm0.2	55.3\pm0.7	52.8\pm0.4	cont.																
+STAG		69.2\pm0.0	40.3\pm0.0	59.9\pm0.0	57.9\pm0.0	69.5\pm0.0	40.4\pm0.0	60.2\pm0.0	58.1\pm0.0	69.7\pm0.0	40.4\pm0.0	60.4\pm0.0	58.2\pm0.0	69.8\pm0.0	40.4\pm0.0	60.6\pm0.0	58.2\pm0.0	70.0\pm0.0	40.3\pm0.0	60.8\pm0.0	58.3\pm0.0	cont.
Round	6	69.1	40.3	59.7	57.8	69.1	40.3	59.7	57.8	69.1	40.3	59.7	57.8	69.1	40.3	59.7	57.8	Avg.				
Source		65.0	34.0	56.6	52.2	64.3	33.0	55.5	51.2	63.5	31.9	54.2	50.2	62.7	30.9	53.2	49.2	62.1	30.1	52.2	48.3	52.4
BN Adapt		62.9\pm0.3	38.7\pm0.2	55.3\pm0.7	52.8\pm0.4	cont.																
+STAG		70.0\pm0.0	40.2\pm0.0	61.0\pm0.0	58.3\pm0.0	70.1\pm0.0	40.2\pm0.0	61.1\pm0.0	58.3\pm0.0	70.1\pm0.0	40.1\pm0.0	61.2\pm0.0	58.2\pm0.0	70.0\pm0.0	39.9\pm0.0	61.2\pm0.0	58.1\pm0.0	70.0\pm0.0	39.7\pm0.0	61.2\pm0.0	58.0\pm0.0	57.2\pm0.0 (4.8)

Table 10. Hyper-parameter configurations (β_0 and γ) for all experimental settings. We report the initial balancing coefficient β_0 and the decay scale γ for each combination of task, scenario, architecture, and baseline method.

Task	Scenario	Dataset	Model	Baseline Method	β_0	γ
Classification	Mild	ImageNet-C	ResNet50-BN	TENT	100	100
				EATA	25	150
				SAR	50	150
				DeYO	12	100
			ResNet50-GN	EATA	250	100
				SAR	150	100
				DeYO	25	50
	Label Shifts	ImageNet-C	VitBase-LN	TENT	300	50
				EATA	100	100
				SAR	500	50
				DeYO	250	50
			ResNet50-GN	EATA	125	100
				SAR	100	70
				DeYO	25	50
Continual	Mix Shifts	ImageNet-C	VitBase-LN	TENT	70	50
				EATA	100	100
				SAR	250	100
				DeYO	25	50
			ResNet50-GN	EATA	500	100
				SAR	200	1000
				DeYO	25	750
	Batch Size 1	ImageNet-C	VitBase-LN	EATA	100	1500
				SAR	500	1000
				DeYO	50	1000
			ResNet50-GN	EATA	500	10000
				SAR	500	10000
				DeYO	25	10000
Segmentation	Continual	CIFAR-10-C	WideResNet-28	TENT	300	10000
				EATA	500	10000
				SAR	1000	10000
				DeYO	250	10000
				BN Stats Adapt	90	15
				TENT	100	10
	CIFAR-100-C	Cityscapes-ACDC	Segformer-B5	CoTTA	5	10
				EcoTTA ($K = 4$)	30	60
				EcoTTA ($K = 5$)	100	10
				BN Stats Adapt	70	15
				TENT	500	5
				CoTTA	10	400